Journal of Porous Materials (2021) 28:1281–1289
https://doi.org/10.1007/s10934-021-01078-0

Synthesis of composite zeolites composed of SAPO-5 and SAPO-34 and its application in methanol dehydration to light olefins

Yadong Bai[1] · Qinghu Zeng[2] · Jinghui Sun[1] · Qingfeng Song[3] · Lei Tang[1] · Wenwen Zhang[1] · Zhiping Liu[1] · Dahai Pan[1]

Accepted: 2 April 2021 / Published online: 10 April 2021

Abstract
In present work, bi-phases composite zeolites consisting of SAPO-5 and SAPO-34 (named as SSC) are prepared by a traditional hydrothermal way, and characterized by X-ray diffraction (XRD), scanning electron microscopy (SEM), N_2 adsorption–desorption, intelligent gravimetric analyzer (IGA), intrusive mercury technology, and NH_3-TPD techniques. The results display that the crystals in the as-synthesized composites have a hierarchical pore system with a size of about 3–130 nm, which displays a butterfly-like pattern on the crystal faces and runs throughout the whole crystal. Catalytic performances of the as-synthesized SSC catalysts are tested during methanol to olefin (MTO). As compared with a microporous composite catalyst, the hierarchical SSC composite catalyst displays excellent catalytic performances with a prolonged catalytic life and an elevated selectivity for light olefins.

Keywords Hierarchical pores · SAPO-5 · SAPO-34 · Butterfly-like distribution · Methanol to olefins

1 Introduction

Zeolite molecular sieves are important microporous crystals with complex one dimensional to three dimensional microporous systems. Due to the high surface area, adjustable acidity, highly thermal and hydrothermal stability, zeolite molecular sieves have been widely used in the fields of such as catalysis, adsorption, ion-exchange, separation. However, their use is hampered by the small inherent microporous channels, which are subjected to diffusion limitations on reaction rates [1–4] because of the similar size between the involved guest molecules and the micropore diameter where most of the active centers locate. It is well known that an advantageous pore structure for molecular transport should be the one the shorter micropores connected by meso- or/and macropores throughout the whole crystal [4–8]. Mesoporous molecular sieves possess high surface areas, large volumes and wide pore diameters, however, the amorphous pore walls, weak acidity and poor hydrothermal stability have been severely hindering their practical applications [9, 10]. Due to the existence of the above-mentioned problems in a single molecular sieve material, research and development of composite molecular sieves [11–14] have attracted much more attentions of many researchers because of their potential catalytic performance resulting from the combination of different types of pore systems, crystalline characters and acid properties into an identical material.

When two or more molecular sieves are combined together and form the composite materials, it may give the new catalyst a synergies effect [15, 16] and an excellent catalytic performance. Liu et al. [11] designed and prepared a core–shell Y@NY composite zeolite and investigated its catalytic performances using triisopropylbenzene (TIPB) as a probe molecule, where the as-synthesized core–shell zeolite served as a tandem micro-reactor and offered the TIPB reactant molecules with a hierarchically cracking process. Li et al. [12] synthesized a SAPO-34/18 composite zeolite with low acid site density for converting methanol to olefins (MTO), and the as-prepared composite zeolites displayed excellent dehydration performances for a high selectivity of

✉ Zhiping Liu
liuzhiping@tyut.edu.cn

[1] College of Chemistry and Chemical Engineering, Taiyuan University of Technology, 79# West Yingze Street, Taiyuan 030024, China

[2] Xi'an Origin Chemical Technologies Co., Ltd, Xi'an 710061, China

[3] The Northwest Research Institute of Chemical Industry Co., Ltd, Xi'an 710061, China

light olefins and a prolonged catalytic life. MCM-41/Beta composites were successfully synthesized by using a seeding method and a two-step crystallization process, and showed an enhanced activity and selectivity of gasoline fraction in catalytic cracking of waste used palm oil [17].

Although the development of composite molecular sieves [11–16, 18] has attracted the attention of many researchers, and the as-synthesized composite catalysts have shown excellent performances in catalysis, adsorption, separation and other aspects, the synthesis of bi-phase zeolite composite composed of SAPO-34 and SAPO-5 and its application in MTO has rarely reported. SAPO-34 is a typical phosphoaluminate molecular sieve with a CHA topological structure, and has been displaying excellent catalytic performances for higher selectivity to alkenes during the MTO process because of its large cages, small windows and milder acidity [19–21]. Besides giving a shape selectivity of light olefins, the small channel (0.38 nm) also leads to a severe diffusion limitation for the by-products such as large hydrocarbon molecules and coke remaining in the large cages. SAPO-5 molecular sieve is one of the important members of the SAPO series, and has an AFI topological structure with a 12-membered ring one-dimensional pore system [22]. Due to its large pore structure (0.73 nm), highly thermal and hydrothermal stability, and strong acidity, SAPO-5 has been widely used in various fields such as isomerization, alkylation, benzylization and MTO conversion reactions [23]. Undoubtedly, due to the inherent small channels, a diffusion limitation inevitably occurs in a single microporous zeolite crystal involving the catalytic reaction of hydrocarbon. The guest molecules hardly escape from the small micropores timely, and are prone to suffer from a secondary reaction, which results in oligomers or carbon deposition [6–8] in the microporous channels, and thus significantly shortens the catalyst life.

Besides different pore structures and acid sites were reported to be integrated into one composite zeolite catalyst, an intercrystalline or intracrystalline meso- or/and macroporous structure, which is caused by different orientations of the bi-phases zeolite [11, 24] or by the framework destruction [1, 6, 25, 26], was also created in the as-synthesized zeolite composites. It is no doubt that the additionally generated meso- or/and macroporous structure not only can solve the problems of diffusion limitation very well by providing a high-speed transport channel for reactants and products, but also can dramatically improve the acid sites accessibility to the guest molecules. In the present work, a bi-phase composite zeolites composed of SAPO-5 and SAPO-34 is synthesized, and a hierarchical pore structure with a 3–130 nm is introduced into the as-synthesized composite zeolites. In order to investigate the catalytic performances of the as-synthesized bi-phases composite catalyst, methanol to olefins (MTO) is used as a probe reaction.

2 Experiment section

2.1 Chemicals

Pseudo-boehmite (70% Al_2O_3) was purchased from Zibo Furao Industry and Trade Co. Ltd, China; Phosphoric acid (85%) was provided by Tianjin Kemio Chemical Reagent Company, China; Tetraethyl ammonium hydroxide (TEAOH, 25 wt%) and triethylamine (TEA) were purchased from Guangfu Chemical Reagent Company, China; Silica sol (25% SiO_2) was offered by Qingdao Ocean Reagent Factory, China. All the materials are directly used without further treatment.

2.2 Catalyst preparation

Pseudo-boehmite, phosphoric acid, and silica sol were used as aluminum source, phosphorus source, silicon source, respectively. TEAOH and TEA served as a mixed structure-directing agent. The molar composition of the reaction mixture was 1.0 Al_2O_3:1.0 P_2O_5: x SiO_2: 0.05 TEAOH: 2.15 TEA: 60 H_2O. Typically, 9.7 g of pseudo-boehmite was dispersed in 47 mL of distilled water. Then 7.7 g of phosphoric acid, 1.96 g of TEAOH, 14.5 g of TEA, and 1.7 g of silica sol were successively added the aforementioned mixture system, and kept continuously stirring at room temperature for 2.5 h. After that, the prepared gel was transferred into a 100 mL stainless steel reaction kettle lined with polytetrafluoroethylene, and then statically crystallized at 200 ℃ for 24 h under autogenous pressure in a thermostatic chamber. After crystallization, the samples were cooled to room temperature, washed to be neutral, and kept drying at 100 ℃ for 6 h. After removing the template agent at a constant temperature of 2 ℃/min to 550 ℃ keeping for 6 h, the as-synthesized samples were collected and denoted as SSC-x, here, the "x" is 0.10, 0.15, and 0.30, respectively.

2.3 Catalyst characterization

X-ray powder diffraction (XRD) patterns were obtained on a Shimadzu LabX XRD-6000 diffractometer, with CuKα radiation at 40 kV and 30 mA, 0.02° step, 8 degree/min. Scanning electron microscopy (SEM) images were taken on a Hitachi S-4800 instrument at an accelerating voltage of 1 kV. Nitrogen adsorption–desorption analysis at a liquid nitrogen temperature (77 K) was determined on a Quantachrome Quadrasorb SI sorption analyzer. Mesopore size distribution is calculated using the Barrett-Joyner-Halenda (BJH) pore size model, as applied to the adsorption branch of the isotherm, and microporous structure was obtained from the t-plot analysis of the adsorption branch of the

isotherm. Macropore size distribution was studied with an AUTOPORE IV 9500 intrusive mercury apparatus. Temperature-programmed desorption of ammonia (NH_3-TPD) was executed on AutochemΠ 2920 apparatus with thermal conductivity detector (TCD).

CH_4 and CO_2 adsorption of the samples at 25 ℃ were investigated by using a Hiden IGA 003 electronic microbalance. The catalyst was outgassed under a vacuum of $< 10^{-3}$ Pa at 400 ℃ for more than 10 h prior to the adsorption measurement. The sample temperature was regulated to ± 0.1 ℃ by a water bath. The pressure was determined using two high accuracy Baratron pressure transducers and increased step by step in order to obtain the entire equilibrium adsorption isotherm. For each step, the amount of adsorbate (CH_4 or CO_2) introduced into the system was kept small enough in order to guarantee an isothermal process.

2.4 Catalytic tests

All catalytic experiments were conducted at atmospheric pressure in a fixed-bed micro-reactor apparatus with a quartz tube (i.d. 6 mm). Prior to the experiments, the catalyst (200 mg) with particle size of 20–40 meshes was routinely activated under flowing N_2 (50 ml/min) at 500 ℃ for 2 h and then kept at the desired reaction temperature (450 ℃). Subsequently, reactant (methanol: H_2O = 1:1, *v/v*) was injected into the quartz tube reactor by a micro-injected pump with a constant LHSV of 2.0 h^{-1}. Products were analyzed by an online gas chromatograph with a flame ionization detector (FID) and a HP-PLOT/Q: 30 m × 0.53 mm × 40 μm.

3 Results and discusses

3.1 Synthesis and characterization

Figure 1, Figs. S1 and S2 are the XRD patterns of the as-synthesized SSC-*x*, SAPO-5, and SAPO-34, respectively. It can be seen from Fig. 1 that all of the as-prepared samples display the characteristic diffraction peaks at about 9.5°, 12.9°, 14.0°, 15.9°, 17.8°, 20.5° and 30.5°, which can be ascribed to the SAPO-34 [5, 8, 26]. The characteristic diffraction peaks at about 7.5°, 14.9°, and 22.4° attributing to SAPO-5 [22, 23] can be seen also in the XRD patterns of the three samples. The aforementioned results suggest the co-existence of CHA and AFI topological structures in the as-synthesized samples.

Figure 1 also shows that with the increase of SiO_2/Al_2O_3 ratios in the gel precursors, the diffraction peaks at about 7.5° and 22.4° attributing to SAPO-5 zeolite phase are obviously weakened while the diffraction peaks at 9.5°, 15.9° and 20.5° belonging to SAPO-34 zeolite phase are elevated accordingly. That may mean that a gel precursor with a higher Si/Al ratio is more prone to the formation of SAPO-34 because more silicon islands [22] are inserted into the as-synthesized zeolite crystals by replacing Al or P species. It is known that during the synthesis of SAPO, the CHA and AFI structures compete with each other [27, 28] and the content of CHA increases with an increase of heteroatoms for example the Si [27].

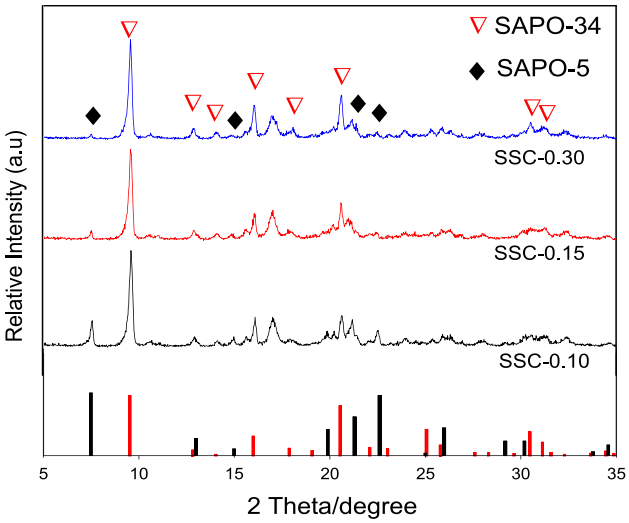

Fig. 1 XRD patterns of the as-synthesized SSC-*x* samples

As shown in Figs. S3 and S4, the pure SAPO-34 and SAPO-5 are cubic-like and hexagonal-like crystals, respectively [27]. It can be inferred from Fig. 2 that except for some irregular amorphous debris, only one kind of cubic crystals can be observed in the as-synthesized samples. Combining with the results as detected by XRD patterns as shown in Fig. 1, the only one kind of cubic crystal in the as-synthesized samples suggests that the SAPO-5 and SAPO-34 are fused into one and form composite zeolites [11, 16, 24, 25]. It can be seen from Fig. 2 that with the increase of SiO_2/Al_2O_3 ratios in the gel precursor, the crystals in the as-made samples show more regular morphologies and have less amorphous debris, suggesting an enhanced crystallinity with an increased Si-species in the gel precursors. When the SiO_2:Al_2O_3 in the synthetic gel is controlled as 0.10:1.0, many loosely irregular debris attributing to small amorphous particles can be obviously observed in the as-synthesized sample SSC-0.10 (Fig. 2a). Moreover, it can be seen from Fig. 2b that the crystals in SSC-0.10 sample display a sponge-like morphology, and a large number of fine holes are obviously observed throughout the whole crystals. When SiO_2/Al_2O_3 ratio in the gel precursors is adjusted as 0.15, the aforementioned loose and irregular amorphous debris are difficult to be detected in SSC-0.15 sample. It can be seen from Fig. 2c that most of the crystals in SSC-0.15 sample are cubes with a relatively smooth surface. While many fine holes, which display a butterfly-like pattern [12, 29] on the

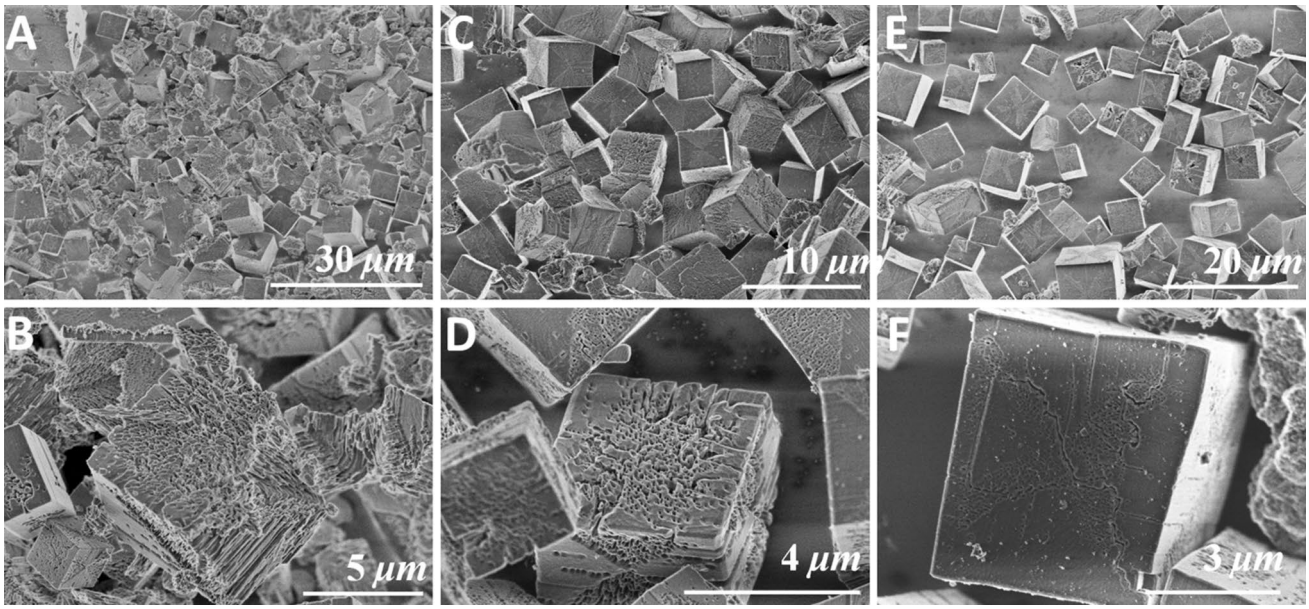

Fig. 2 SEM images of the as-synthesized SSC-*x* composite zeolites. **a**, **b** SSC-0.10; **c**, **d**: SSC-0.15; **e**, **f** SSC-0.30

external surfaces of the crystals, can be observed in SSC-0.15 sample also (Fig. 2d). The crystals in the samples SSC-0.30 yielded from a gel precursor with a SiO_2/Al_2O_3 ratio of 0.30 have a more regular cubic morphology and rather smooth external surfaces. Furthermore, the butterfly-like distribution fine holes can hardly be detected on the external surface of the crystals in the SSC-0.30 sample (Fig. 2e–f).

It can be inferred from Figs. 1 and 2 that the reduced holes on the crystal faces show a positive correction with the decreased SAPO-5 zeolite phase in the composite zeolites. An increased SiO_2/Al_2O_3 ratio in the gel precursors not only leads to a decreased SAPO-5 zeolite phase in the composite (Fig. 1), but also leads to a reduced number of the holes on the crystal surfaces (Fig. 2). Combining with the results of Figs. 1 and 2, it would suggest that butterfly-like distribution portion in the crystal may belong to SAPO-5 zeolite phase, and the other part in the cubic crystal should be SAPO-34 zeolite phase. The only one kind of crystal morphology as observed by the SEM images as shown in Fig. 2b, d and f also strongly suggests that the SAPO-5 and SAPO-34 zeolite phases in SSC-0.10, SSC-0.15 and SSC-0.30 are not simply physically mixed.

Figure 3 shows the nitrogen adsorption–desorption isotherms of the Na-form samples and the corresponding BJH

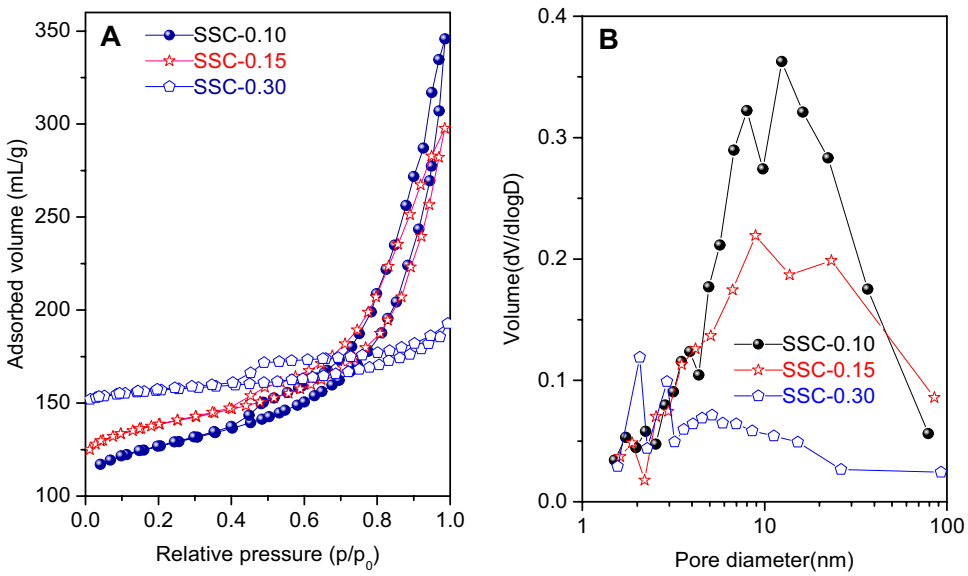

Fig. 3 N_2 adsorption–desorption isotherms of the samples (**a**), and the corresponding BJH pore size distribution curves (**b**)

Table 1 Physical structural properties of samples

Samples	S_{BET} (m^2/g)	S_{mic} (m^2/g)	S_{ext} (m^2/g)	V_{mic} (cm^3/g)	V_{meso} (cm^3/g)
SSC-0.10	739	583	156	0.23	0.26
SSC-0.15	746	609	137	0.25	0.21
SSC-0.30	705	664	41	0.28	0.07

pore distribution curves. As shown in Fig. 3a, SSC-0.30 zeolite has a type-I isotherm (similar to the ones of the single SAPO-5 and SAPO-34 samples as shown in Fig. S5a) with a small H3 hysteresis loop, indicating the presence of micropore mainly [29]. However, both of SSC-0.15 and SSC-0.10 zeolite composite exhibit the curves combining type-I and type-IV isotherms with big hysteresis loops combining H3 and H4, indicating the co-existence of micropores and mesopores in the as-synthesized samples [4–8, 30, 31]. The BJH pore size distribution (Fig. 3b) derived from the adsorption branch [4, 5, 11] of the isotherm of the samples illustrates the existence of mesopore structure with a pore size distribution ranging from 2 to 80 nm, while the similar pore size distribution is not observed in the sample of SSC-0.30 as well as the single SAPO-5 and SAPO-34 sample (Fig. S5b).

Table 1 shows the pore structure parameters of different samples. Sample SSC-0.30 has the largest micropore area and micropore volume, which is attributed to its high crystallinity and relatively intact and regular crystal particles as shown in Fig. 2. It is difficult to see the loose and irregular debris as detected in SSC-0.10 sample, indicating that the crystal in SSC-0.30 is more perfect. Fewer lattice defects mean a higher order [2]. Table 1 also shows that although the micropore area and micropore volume of the synthesized SSC-0.10 and SSC-0.15 samples decrease with different degrees, the BET surface area and mesoporous volume significantly increases. As compared with SSC-0.30, the micropore area of samples SSC-0.10 and SSC-0.15 respectively decreases by 81 m^2/g and 55 m^2/g, while the external surface area increases by 115 m^2/g and 96 m^2/g, respectively. Furthermore, the micropore volume of SSC-0.10 and SSC-0.15 respectively decreases by 0.05 cm^3/g and 0.03 cm^3/g, but the corresponding mesopore volume increases by 0.19 cm^3/g and 0.14 cm^3/g, respectively. The abovementioned results display that due to the introduction of mesoporous structure, additional mesoporous area and volume can be obtained by slightly sacrificing the micropore properties.

In order to further reveal the created "secondary" pore structure, the as-synthesized SSC-0.10 sample was crushed before SEM observation, and the subsequent electron microscopic observed result is shown in Fig. 4. After being crushed by 20 MPa, part of the crystals are broken, which can make a more intuitive observation of the internal structure of the zeolite crystals. It can be inferred that the introduced meso- and macropore structure goes throughout the whole zeolite crystal. As shown in Fig. 5, indirect evidence for the presence of macropore structure is also provided by the intrusive mercury experiment. The pore size distribution of the as-synthesized SSC-0.10 illustrates the existence of a macropore structure with pore size centering at about 80 nm, which is in good agreement with the results observed by SEM and nitrogen adsorption–desorption experiment. Combining with the mesopore distribution decided by DFT

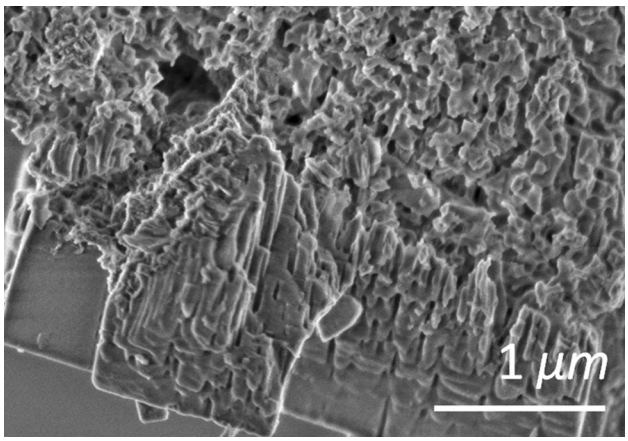

Fig. 4 SEM images of SSC-0.10 after crushed by 20 MPa pressure

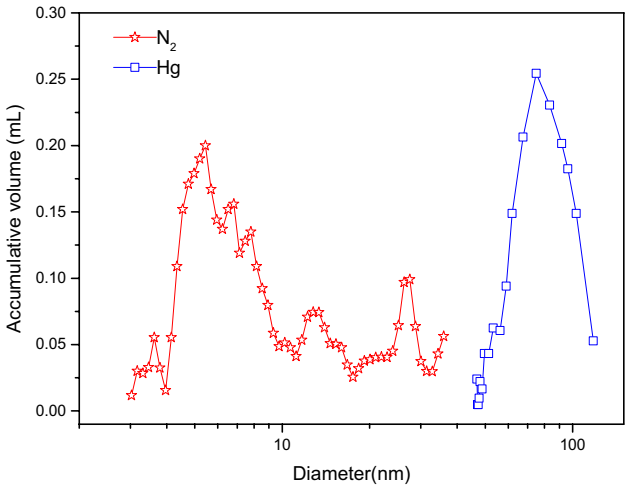

Fig. 5 The created hierarchical pore system in the as-synthesized sample SSC-0.10. (☆) mesopore structure (DFT pore size distribution curves obtained from the N2 adsorption isotherms) and (□) macropore structure decided by intrusive mercury technology

model (slightly different from that obtained by BJH model), a hierarchical pore system with a size of about 3 ~ 130 nm is therefore introduced into the as-synthesized sample SSC-0.10 (Fig. 5).

Figure 6 is the NH_3-TPD curves of the as-synthesized samples. It can be seen that all samples have two desorption peaks, one at 213–221 ℃ and the other at about 409–433 ℃, which should be ascribed to the ammonia desorption from weak and strong acid sites, respectively [8, 12]. It can be inferred from Fig. 6 that the three samples have different acid properties: with the increase of "*x*" in the sample SSC-*x* (0.10, 0.15, 0.30), the acid amount of the samples increases accordingly, and the corresponding peak position of desorption NH_3 from the strong acid sites moves toward a high temperature region, not only indicating the total acid amount but also suggesting the acid strength increases with the elevated Si/Al ratios [12].

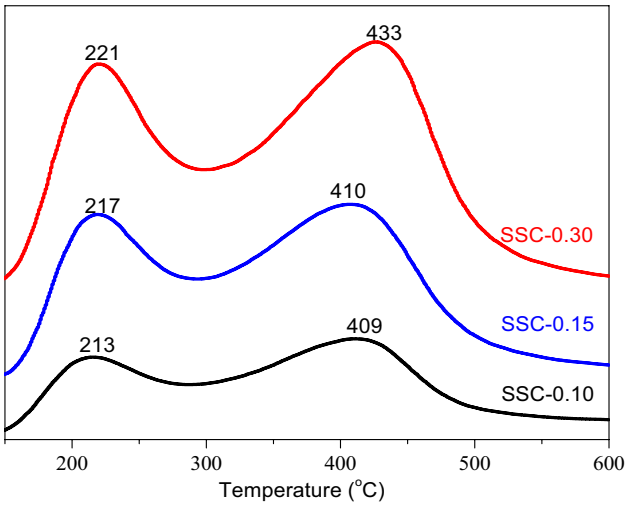

Fig. 6 NH_3-TPD curves of the as-synthesized samples

3.2 Adsorption of CO_2 and CH_4

Guest molecules CO_2 and CH_4 may suffer from different diffusion limitation and display different adsorption properties in the small micropores of SAPO-34 zeolite [32]. SAPO-34 has been therefore widely used in the CO_2/CH_4 separation process [32, 33]. As shown in Fig. 7, at room temperature and under the same partial pressure, the adsorption amount of CH_4 or CO_2 on SSC-0.10 significantly decreases as compared with those on SSC-0.30, indicating that the mesoporous structure created in the samples does not contribute to the increase of CO_2 or CH_4 adsorption amount. As shown in Fig. 7, the adsorption amount of CO_2 and CH_4 on SSC-0.30 is about 21.5% and 15.0% higher than those on the SSC-0.10, respectively, indicating that the adsorption mainly occurs in micropores. It can be seen in Table 1, the BET specific surface area, total pore volume and mesoporous volume of SSC-0.10 is significantly higher than those of SSC-0.30, while the micropore volume of SSC-0.30 is about 21.7% higher than that of SSC-0.10, further suggesting that the micropores of the adsorbent are the main adsorption spaces. Figure 7 also shows that CH_4 adsorption on SSC-0.10 and SSC-0.30 increases rapidly with the increase of relative pressure, while the adsorbed CO_2 increases slowly with the increased relative pressure of adsorbate. That reflects CH_4 adsorption in the two adsorbents is more sensitive with the increase adsorbate pressure.

3.3 Catalytic tests

SAPO is a kind of advantageous catalyst in MTO (methanol to olefins) reaction [19–21, 26]. However, this catalyst deactivates rapidly because of carbon deposition in the micropore channel during the methanol dehydration. The carbon deposition on the external surfaces or in the micropores can increase the transport resistance of

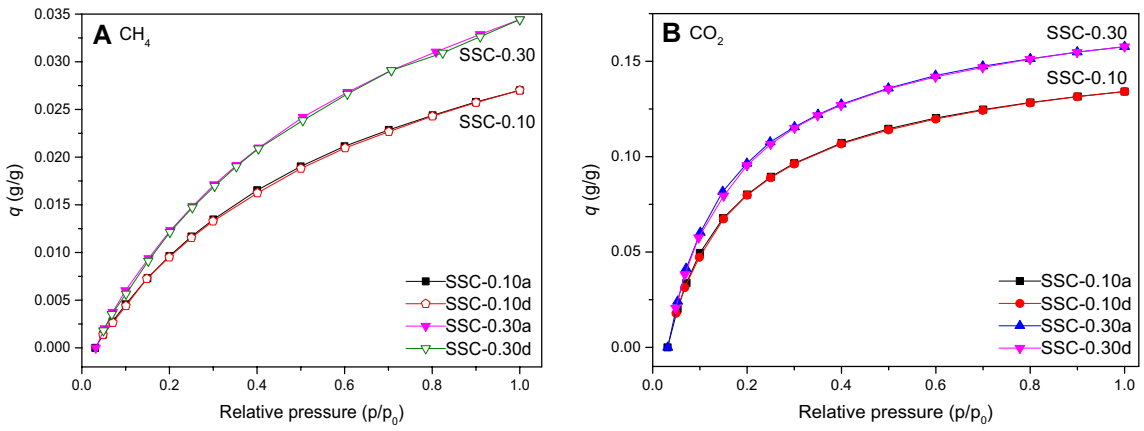

Fig. 7 Adsorption performances of the as-synthesized samples at 25 ℃. **a** CH_4 adsorption–desorption isotherms **b** CO_2 adsorption–desorption isotherms

reactant or product molecules, and even lead to a rapid deactivation of the catalyst, which hinders their practical applications. The created hierarchical pore system can effectively shorten the length of the micropore channels, which may be conducive to the fast escape of the coking precursor from the micropores and can thus offer the catalysts excellent catalytic performances [26].

As shown in Fig. 8a, all the catalysts display a 100% initial conversion of methanol while a different stability. After 3.5 h with the time on stream, the conversion of methanol over the SSC-0.30 catalyst decreases from 100 to 96.7%. However, it respectively takes the SSC-0.15 and SSC-0.10 catalysts about 6.5 h and 7.5 h to have the similar conversion. Obviously, as compared with SSC-0.30,

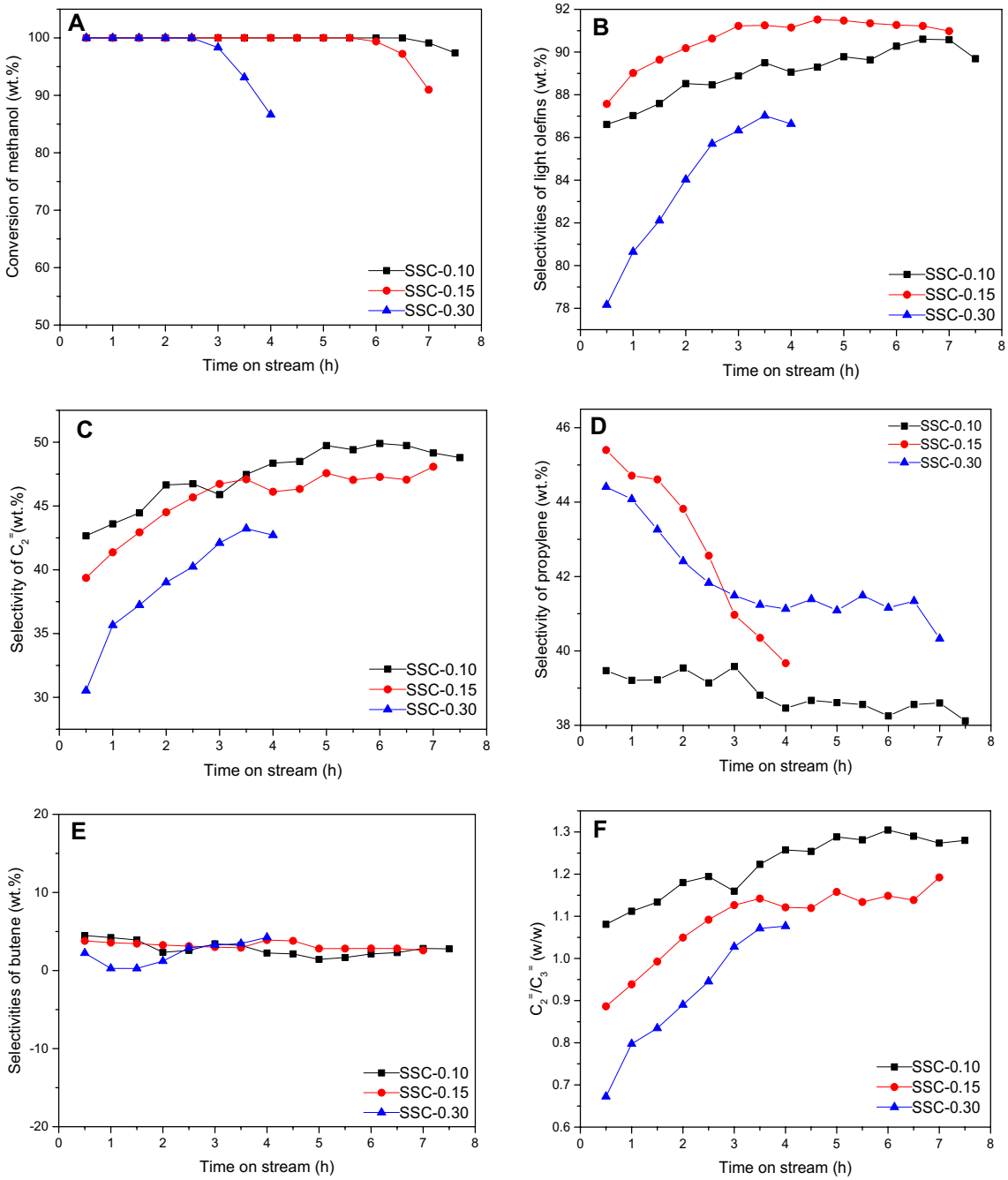

Fig. 8 Methanol to olefins over the different catalysts: **a** The conversion of methanol; **b** The selectivity of light olefins ($C_2^=$, $C_3^=$ and $C_4^=$) with the time on stream. **c** The selectivity of the ethylene; **d** The selectivity of propylene; **e** The selectivity of butane; **f** The $C_2^=/C_3^=$ ratios (*w/w*) over the different catalysts related with the time on stream

catalysts SSC-0.10 and SSC-0.15 are more stable. The increased stability of SSC-0.10 and SSC-0.15 should be attributed to the introduced hierarchically porous structure [5].The created meso or macroporous structure effectively shortens the length of the microporous channels and significantly increases the number of pore windows [2]. That is not only conducive to the rapid diffusion of reactants and products, but also beneficial to the deposition carbon precursors escaping from the micropores [5, 34, 35], which avoids rapid deactivation of catalysts. The weaker acid strength and lower acid density in SSC-0.10 catalyst (Fig. 6), especially the weakened strong acid sites, may also play a role in extending the catalyst life.

When SAPO is used as a catalyst during a methanol dehydration reaction, scientists have been devoting themselves to elevating the selectivity of light olefin [26, 36]. During an MTO process, in addition to ethylene, propylene and butylene, a small amount of methane, ethane, paraffin hydrocarbon and aromatic hydrocarbon are often detected [36]. Moreover, DME is also observed at later period. Figure 8b shows that the selectivity of tri-olefins ($C_2^=$, $C_3^=$, and $C_4^=$) increases firstly and then decreases with the time on stream. We know that the light olefins can be deemed as intermediate products during the MTO process, and they are largely affected by the acid properties and porous structure of the dehydration catalysts [5]. With the prolonged reaction time, partial acid centers in the catalyst are covered by deposition carbon, and the acid sites density is reduced accordingly, which depresses the olefins oligomerization; while an excessively weakened acidity may also depress the formation of olefin but contribute to the formation of DME. The selectivity of tri-olefins on the hierarchical zeolite SSC-0.10 and SSC-0.15 is higher than that on the microporous SSC-0.30. It can be seen from Fig. 8b that the highest selectivity of light olefins on SSC-0.30 is 87.0%, while those on SSC-0.10 and SSC-0.15 are 90.6% and 91.4%, respectively. It can be seen from Fig. 8c–e that despite of the similar selectivity of butene, the hierarchical composite zeolites catalysts SSC-0.10 and SSC-0.15 have higher selectivity of ethylene while lower propylene selectivity. More light olefins detected on the hierarchical zeolite catalysts should be attributed to the weakened acidity (Fig. 6). Furthermore, the introduction of hierarchical pore structure can help the generated light olefins escaping from pores rapidly, which depresses the oligomerization of olefins, not only helping to improve the stability of the catalyst, but also helping to increase the selectivity of the light olefin [12, 26]. With the prolonged reaction time, the selectivity of ethylene on all catalysts significantly increases, while the selectivity of propylene slightly decreases. The overlaying result led to the increased $C_2^=/C_3^=$ ratio with an extended reaction time (Fig. 8f).

4 Conclusion

Bi-phases composite zeolites composed of SAPO-5 and SAPO-34 were synthesized. XRD indicated that the proportion of SAPO-34 zeolite phase in the composite increased with the increased silicon species in the gel precursors. SEM results showed that the SAPO-5 and SAPO-34 coexisted in the cubic crystals, and abundant holes with butterfly-like distribution were observed on the crystal surface of the as-synthesized samples. Nitrogen adsorption–desorption and intrusive mercury technology results exhibited that a hierarchical pore system with a pore distribution of 3–130 nm was built in the as-synthesized SSC-0.10 and SSC-0.15 samples. CH_4 and CO_2 adsorption experiments showed that the introduced hierarchical pore structure could not increase the adsorption amount, indicating that the adsorption behavior of this kind of gas mainly occurred in the micropores. During the catalytic reaction of methanol dehydration to olefins, the created hierarchically porous structure significantly improved the stability of the catalyst. As compared to the microporous SSC-0.30, the hierarchical composite SSC-x ($x = 0.10, 0.15$) catalyst has a much higher ethylene selectivity. Such a synthesis route may offer a potential excellent catalyst for methanol dehydration to light olefins.

Supplementary Information The online version contains supplementary material available at https://doi.org/10.1007/s10934-021-01078-0.

Acknowledgements This work is supported by NSFC (21975174, 21706177), National Key R&D Program of China (2020YFB0606405) and SinoPEC (116050).

References

1. J. Pérez-Ramírez, C.H. Christensen, K. Egeblad, C.H. Christensend, J.C. Groen, Hierarchical zeolites: enhanced utilisation of microporous crystals in catalysis by advances in materials design. Chem. Soc. Rev. **37**, 2530 (2008)
2. Y.S. Tao, H. Kanoh, K. Kaneko, Synthesis of mesoporous zeolite A by resorcinol-formaldehyde aerogel templating. Langmuir **21**, 504 (2005)
3. S. van Donk, A.H. Janssen, J.H. Bitter, K.P. de Jong, Generation, characterization, and impact of mespores in zeolite catalysts. Catal. Rev. Sci. Eng. **45**, 297 (2003)
4. L.C. Zhang, X.B. Sun, M. Pan, X.N. Yang, Y.C. Liu, J.H. Sun, Q.H. Wang, J.J. Zheng, Y. Wang, J.H. Ma, W.L. Li, R.F. Li, Interfacial effects between carbon nanotube templates and precursors on fabricating a wall-crystallized hierarchical pore system in zeolite crystals. J. Mater. Sci. **55**, 10412–10426 (2020)
5. X.Y. Cui, J.J. Wang, M. Pan, W.W. Ning, L.L. Yan, J.J. Zheng, R.F. Li, Hierarchical SAPO-34: Synthesis and Catalytic Performances in Methanol to Olefins. Chin. J. Inor. Chem. **34**(2), 300–308 (2018)
6. D. Verboekend, J. Pérez-Ramírez, Design of hierarchical zeolite catalysts by desilication. Catal. Sci. Technol. **1**(6), 879–890 (2011)

7. L. Wu, V. Degirmenci, P.C.M.M. Magusin, N.J.H.G.M. Lousberg, E.J.M. Hensen, Mesoporous SSZ-13 zeolite prepared by a dual-template method with improved performance in the methanol-to-olefins reaction. J. Catal. **298**, 27–40 (2013)
8. A.K. Singh, R. Yadav, A. Sakthivel, Synthesis, characterization, and catalytic application of mesoporous SAPO-34 (MESO-SAPO-34) molecular sieves. Micropor. Mesopor. Mater. **181**, 166–174 (2013)
9. A. Sayari, Catalysis by crystalline mesoporous molecular sieves. Chem. Mater. **8**(8), 1840–1852 (1996)
10. A. Corma, From microporous to mesoporous molecular sieve materials and their use in catalysis. Chem. Rev. **97**(6), 2373–2420 (1997)
11. Y.C. Liu, B. Qin, H.X. Gao, W.W. Ning, L.C. Zhang, J.J. Zheng, Y.Z. Du, Y. Wang, W.L. Li, R.F. Li, Core-shell Y zeolite with a mono-crystalline core and a loosely aggregating polycrystalline shell: a hierarchically cracking catalyst for large reactants. Catal. Sci. Technol. **10**, 2303–2312 (2020)
12. Y.X. Li, Y.H. Huang, J.H. Guo, M.Y. Zhang, D.Z. Wang, F. Wei, Y. Wang, Hierarchical SAPO-34/18 zeolite with low acid site density for converting methanol to olefins. Catal. Today **233**, 2–7 (2014)
13. S.Y. Liu, H.K. Zhang, H.M. Chen, Z.Q. Chen, L.W. Zhang, J. Ren, X.D. Wen, Y. Yang, Y.-W. Li, Fabrication of core-shell TON@MFI material and its enhanced catalytic performance for toluene alkylation. Catal. Sci. Technol. **10**, 1281–1291 (2020)
14. N. Masoumifard, R. Guillet-Nicolas, F. Kleitz, Synthesis of Engineered Zeolitic Materials: From Classical Zeolites to Hierarchical Core-Shell Materials. Adv. Mater. **30**, 1704439–1704479 (2018)
15. L. Huang, W. Guo, P. Deng, Z. Xue, Q. Li, Investigation of synthesizing mcm-41/zsm-5 composites. J. Phy. Chem. B **104**(13), 2817–2823 (2000)
16. J.J. Zheng, X.W. Zhang, Y. Wang, Y.D. Bai, W.F. Sun, R.F. Li, Synthesis and catalytic performance of a bi-phase core-shell zeolite composite. J. Porous Mater. **16**, 731–736 (2009)
17. Y.S. Ooi, R. Zakaria, A.R. Mohamed, S. Bhatia, Synthesis of composite material mcm-41/beta and its catalytic performance in waste used palm oil cracking. Appl. Catal. A Gen. **274**(1–2), 15–23 (2004)
18. X. Li, F. Rezaei, D.K. Ludlow, A.A. Rownaghi, Synthesis of SAPO-34@ZSM-5 and SAPO-34@Silicalite-1 Core−Shell Zeolite Composites for Ethanol Dehydration. Ind. Eng. Chem. Res. **57**, 1446–1453 (2018)
19. U. Olsbye, S. Svelle, M. Bj ø rgen, P. Beato, T.V.W. Janssens, F. Joensen, S. Bordiga, K.P. Lillerud, Conversion of methanol to hydrocarbons: how zeolite cavity and pore size controls product selectivity. Angew. Chem. Int. Ed. **51**(24), 5810–5831 (2012)
20. J. Li, Y.X. Wei, J.R. Chen, S.T. Xu, Z. Liu, Cavity controls the selectivity: insights of confinement effects on MTO reaction. ACS Catal. **5**(2), 661–665 (2014)
21. S. Teketel, L.F. Lundegaard, W. Skistad, S.M. Chavan, U. Olsbye, K.P. Lillerud, P. Beato, S. Svelle, Morphology-induced shape selectivity in zeolite catalysis. J. Catal. **327**, 22–32 (2015)
22. G. Sastre, D.W. Lewis, C.R.A. Catlow, Modeling of Silicon Substitution in SAPO-5 and SAPO-34 Molecular Sieves. J. Phy. Chem. B **101**(27), 5249–5262 (1997)
23. J.M. Campelo, F. Lafont, J.M. Marinas, Pt/sapo-5 and pt/sapo-11 as catalysts for the hydroisomerization and hydrocracking of n-octane. J. Chem. Soc. Faraday Trans. **91**(10), 1551 (1995)
24. J.J. Zheng, X.B. Sun, Y.Z. Du, B. Qin, Y.Y. Zhang, H.Y. Zhang, M. Pan, R.F. Li, Structural features of core-shell zeolite-zeolite composite and its performance for methanol conversion into gasoline and diesel. J. Mater. Res. **31**(15), 2302–2316 (2016)
25. G.S. Wang, Y.J. Liu, J.J. Zheng, M. Pan, H.Y. Zhang, B. Li, S. Yuan, Y.M. Yi, H.P. Tian, R.F. Li, Zeolite-zeolite composite fabricated by polycrystalline Y zeolite crystals parasitizing ZSM-5 zeolite. J. Mater. Res. **30**(16), 2434–2446 (2015)
26. X.X. Chen, D.Y. Xi, Q.M. Sun, N. Wang, Z.Y. Dai, D. Fan, V. Valtchev, J.H. Yu, A top-down approach to hierarchical sapo-34 zeolites with improved selectivity of olefin. Micropor. Mesopor. Mater. **234**, 401–408 (2016)
27. S.H. Jhung, J.S. Chang, J.S. Hwang, S.E. Park, Selective formation of sapo-5 and sapo-34 molecular sieves with microwave irradiation and hydrothermal heating. Micropor. Mesopor. Mater. **64**(1), 33–39 (2003)
28. P. Concepción, J.M. López Nieto, A. Mifsud, J. Pérez-Pariente, Preparation and characterization of Mg-containing AFI and chabazite-type materials. Zeolites **16**(1), 56–64 (1996)
29. J. Gong, F. Tong, X.B. Ji, C.F. Zeng, C.Q. Wang, Y.N. Lv, L.X. Zhang, Hollow SAPO-34 Cubes with Hierarchically Organized Internal Structure. Cryst. Growth Des. **14**(8), 3857–3863 (2014)
30. T.M. Neves, J.O. Fernandes, L.M. Lião, E.D. da Silva, C.A. da Rosa, V.B. Mortola, Glycerol dehydration over micro- and mesoporous ZSM-5 synthesized from a one-step method. Micropor. Mesopor. Mater. **275**, 244–252 (2019)
31. H.B. Zhang, Z.J. Hu, L. Huang, H.X. Zhang, K.S. Song, L. Wang, Z.P. Shi, J.X. Ma, Y. Zhuang, W. Shen, Y.H. Zhang, H.L. Xu, Y. Tang, Dehydration of glycerol to acrolein over hierarchical ZSM-5 zeolites: effects of mesoporosity and acidity. ACS Catal. **5**, 2548–2558 (2015)
32. M.A. Carreon, S.G. Li, J.L. Falconer, R.D. Noble, Alumina-supported SAPO-34 membranes for CO_2/CH_4 separation. J. Am Chem. Soc. **130**(16), 5412–5413 (2008)
33. S. Li, G. Alvarado, R.D. Noble, J.L. Falconer, Effects of impurities on CO_2/CH_4 separations through SAPO-34 membranes. J. Membrane Sci. **251**(1–2), 59–66 (2005)
34. A. Martínez, E. Peris, M. Derewinski, A. Burkat-Dulak, Improvement of catalyst stability during methane dehydroaromatization (MDA) on Mo/HZSM-5 comprising intracrystalline mesopores. Catal. Today **169**(1), 75–84 (2011)
35. X. Wang, Y. Li, C. Luo, B. Chen, Direct synthesis of hierarchical zeolites with oriented nanocrystals without adding extra templates. RSC Adv. **3**(18), 6295–6298 (2013)
36. S. Wilson, P. Barger, The characteristics of SAPO-34 which influence the conversion of methanol to light olefins. Micropor. Mesopor. Mater. **29**(1–2), 117–126 (1999)